AGU PUBLICATIONS

JGR

Journal of Geophysical Research: Atmospheres

RESEARCH ARTICLE
10.1002/2016JD025187

**Key Points:**
- The sensitivity of soil moisture and surface water balance to soil type depends on aridity
- Modeled soil moisture, evapotranspiration, and flood index are most sensitive in humid, transitional, and arid regions, respectively
- Models with a groundwater component show greater sensitivities to soil type than those without a groundwater component

**Correspondence to:**
Z.-L. Yang,
liang@jsg.utexas.edu

**Citation:**
Zheng, H., and Z.-L. Yang (2016), Effects of soil-type datasets on regional terrestrial water cycle simulations under different climatic regimes, *J. Geophys. Res. Atmos.*, *121*, 14,387–14,402, doi:10.1002/2016JD025187.

Received 5 APR 2016
Accepted 12 NOV 2016
Accepted article online 16 NOV 2016
Published online 22 DEC 2016



# Effects of soil-type datasets on regional terrestrial water cycle simulations under different climatic regimes

**H. Zheng**[1] **and Z.-L. Yang**[1,2]

[1]Key Laboratory of Regional Climate-Environment Research for Temperate East Asia, Institute of Atmospheric Physics, Chinese Academy of Sciences, Beijing, China, [2]Department of Geological Sciences, The John A. and Katherine G. Jackson School of Geosciences, University of Texas at Austin, Austin, Texas, USA

**Abstract** Hydrological simulations play an important role in estimating terrestrial water budgets and monitoring extreme events such as floods. This study investigates how these simulations are affected by soil-type datasets and characterizes how these effects vary with climate. We study the differences between two ensemble simulations in China with the Noah-MP land surface model using two soil datasets from the Food and Agriculture Organization and Beijing Normal University. The differences in ensemble means are analyzed over a 10 year period from 2003 to 2012 with respect to estimated soil moisture, the partition of precipitation between evapotranspiration and runoff, and a flood magnitude index. Results show that the hydrological simulations using sandier soil types result in lower soil moisture, lower evapotranspiration, and higher subsurface runoff. Each of these effects varies uniquely with aridity. The changes in soil moisture decrease with increasing aridity, while the changes in water balance components (evapotranspiration and runoff) peak in the transitional zone between humid and arid regions. The flood magnitude, expressed as the maximum daily flow normalized by annual flow, is also substantially influenced by the input soil type. Soil types with more clay and less sand content yield significantly bigger floods, especially in arid regions.

## 1. Introduction

Soil moisture, evapotranspiration, and runoff are all important variables for understanding the terrestrial water cycle. Soil moisture is a major component of terrestrial water storage and constrains the partitioning of precipitation into evapotranspiration and runoff [*Seneviratne et al*., 2010]. By supplying water from the land surface to the atmosphere, evapotranspiration substantially impacts cloud formation and precipitation [*Wang and Dickinson*, 2012]. As part of the precipitation that does not evaporate or infiltrate the soil, runoff coalesces into river flows and is a primary water source for agricultural irrigation [*Rost et al*., 2008]. Floods, which are extreme runoff events, are a major natural hazard to society [*Hirabayashi et al*., 2013].

Land surface models (LSMs) provide a systematic approach to monitoring the geographic distributions and temporal variations of these variables, and hence, these models have been frequently used to predict droughts and floods [*Xia et al*., 2014; *Wood et al*., 2015]. However, the simulations using LSMs experience significant uncertainties, which are attributed to atmospheric forcing [*Wang and Zeng*, 2011; *Liu and Xie*, 2013], parameterization schemes [*Gao et al*., 2015; *Zheng et al*., 2016], vegetation conditions [*Zhang et al*., 2001], and the assumptions of soil properties [*Richter et al*., 2004; *Xia et al*., 2015].

Because of the lack of sufficient soil surveys, the representation of soil is a major source of modeling uncertainty [*Bastidas et al*., 2006; *Shi et al*., 2014]. Several studies have investigated how this uncertainty affects the regional hydrological simulations. *Osborne et al*. [2004] examined the effects of soil texture on regional hydrological simulations and found that soil properties alter the partitioning between surface and subsurface runoff processes. *Livneh et al*. [2015] compared a pair of simulations in the Mississippi River basin using two soil datasets derived from the Harmonized World Soil Database (HWSD) and the State Soil Geographic (STATSGO2) project and showed that the two experiments substantially differ from each other in response to extreme events (floods and droughts). *De Lannoy et al*. [2014] compiled a new soil dataset from the HWSD version 1.21 and the STATSGO2 data. Their revised dataset improves the simulated climatology of soil moisture and surface water fluxes.

However, these studies have not provided generalized conclusions as to how soil types affect soil moisture and the surface water balance across different climates as measured by aridity, a condition that strongly regulates the hydrological processes [*Guo et al*., 2014; *van der Velde et al*., 2014]. In humid regions, annual precipitation is greater than the annual potential evapotranspiration (interpreted as the annual net radiation divided by the latent heat of vaporization for water in this paper following *Arora* [2002] and *Gerrits et al*. [2009]), and runoff is likely to exceed evapotranspiration [*Arora*, 2002]. In arid regions where the annual precipitation is much less than the annual potential evapotranspiration, evapotranspiration dominates over runoff [*Arora*, 2002].

Note that previous studies generally used only a single LSM with an implicit assumption that the sensitivity is the same across different models. However, LSMs behave differently in replicating terrestrial water budgets due to different parameterization schemes, as demonstrated by numerous groups that participated in the Project for Intercomparison of Land surface Parameterization Schemes [*Henderson-Sellers et al*., 1993] and by recent model intercomparisons at continental scales [*Cai et al*., 2014b; *Xia et al*., 2015]. *Bastidas et al*. [2006] showed that such disparity in models' simulations can affect the sensitivity of parameters with similar physical meaning, which was often overlooked in previous studies.

This paper aims to understand the dependency of model sensitivity to soil type on climatic conditions and the consistency of the sensitivity under different parameterization schemes. A pair of numerical experiments are conducted using two soil datasets over China with each pair consisting of an ensemble of 12 Noah with Multiple Parameterizations (Noah-MP) members. Model performance is evaluated using the terrestrial water storage anomaly data released from the Gravity Recovery and Climate Experiment (GRACE) and the evapotranspiration estimate from MOderate Resolution Imaging Spectroradiometer (MODIS). Based on the evaluations, it is analyzed how aridity regulates the model sensitivity of soil moisture climatology, annual mean surface water fluxes, and flood magnitude to soil type. The consistency of the sensitivities across the ensemble members is also addressed.

This paper is organized as follows. Section 2 represents the model and data. Results of the model sensitivity and its consistency under different parameterization schemes are reported in section 3. Sections 4 and 5 provide the discussions and conclusions, respectively.

## 2. Methodology

### 2.1. Soil Datasets

Two datasets of soil type, the Food and Agriculture Organization (FAO) and Beijing Normal University (BNU) datasets, were used. As far as we know, these datasets are the only two publicly available datasets for the countrywide terrestrial water cycle modeling in China. The FAO dataset was derived from FAO/United Nations Educational, Scientific and Cultural Organization Soil Map of the World (SMW) at 1:5,000,000 scale [*Food and Agriculture Organization/United Nations Educational, Scientific and Cultural Organization* (*FAO/UNESCO*), 1971–1981] by *Reynolds et al*. [2000]. The BNU dataset was compiled from the 1:1,000,000 Soil Map of China (SMC) [*Shi et al*., 2004] by *Shangguan et al*. [2012] at Beijing Normal University. The number of soil profiles compiled in the SMW and SMC is substantially different. The SMW consists of only about 60 profiles [*Shangguan et al*., 2012], which are mainly located in northern China [*FAO/UNESCO*, 1971–1981]. However, the SMC consists of about 9000 profiles across China [*Shangguan et al*., 2012] and is thus expected to represent the soil spatial heterogeneity better than the SMW, especially in regions outside of northern China (e.g., the Loess Plateau, northwestern China, and southern China), where the SMW does not contain sufficient systematic soil surveys.

The method of specifying soil type from the original soil texture data (sand and clay content) was adopted from *Reynolds et al*. [2000]. First, gridded sand and clay content was calculated at a 0.25° resolution by area-weighted averaging of the original soil texture data at different spatial resolutions. Then, the sand-clay pairs were classified as the 12 United States Department of Agriculture soil types using the soil texture ternary diagram, which could be used in Noah-MP directly. This method was applied to both the FAO and BNU datasets.

As shown in Figure 1a, the FAO and BNU datasets specify different soil types for 65% of the land area in China. Of the most frequent discrepancies in soil type between the FAO and BNU datasets, three type mismatches cover 40% of China and occur in all climate regions: loam in the FAO dataset and silt loam in the BNU dataset (L-SiL), loam in the FAO dataset and sandy loam in the BNU dataset, and clay loam in the FAO

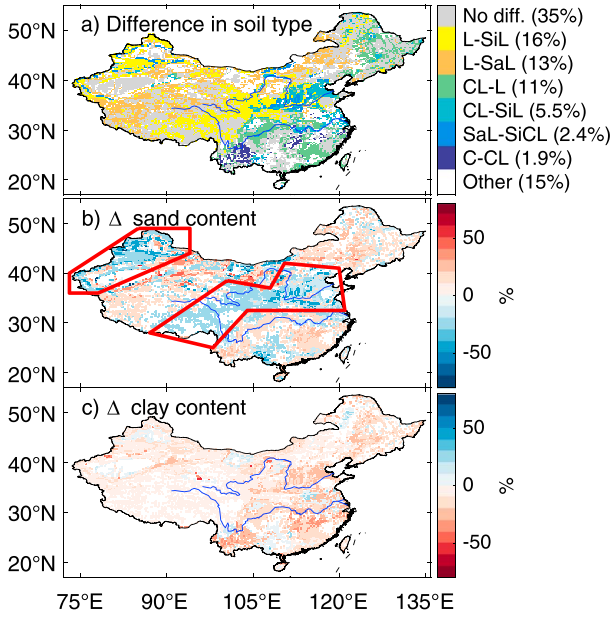


**Figure 1.** Simulation domain and the differences between the BNU and FAO soil-type datasets: (a) difference in soil type, (b) difference in sand content, and (c) difference in clay content. Sa = sand, C = Clay, Si = Silt, and L = Loam. The area fractions of the six most frequent soil-type changes are represented in parentheses.

dataset and loam in the BNU data set. Compared to the FAO, the BNU dataset shows a greater presence of silt in the upper and lower reaches of the Yellow River basin, especially in the Loess Plateau region. This suggests that the BNU dataset has captured the regional soil features characterized by wind-driven silt deposition [*Liu*, 1999]. Figures 1b and 1c show the differences of sand and clay content derived from soil type using the look-up table of *Cosby et al*. [1984]. The BNU dataset implies less sand in both the Yellow River basin and northwestern China (the areas within the red polygons in Figure 1 b), showing more consistency with in situ observations [*Shangguan et al*., 2012]. In southern China and northeastern China, the soil is sandier in the BNU data than in the FAO data. However, a comprehensive evaluation of the two datasets is beyond the scope of this paper as it focused on analyzing the model sensitivities to soil types.

### 2.2. Experimental Design

The Noah LSM with multiple parameterizations (Noah-MP) was used for all simulations. Noah-MP improves over the original Noah in physical realism (now including an interactive vegetation canopy, a multilayer snowpack, and a dynamic groundwater component, among other enhancements) [*Niu et al*., 2011]. The model has been shown to reasonably replicate multiscale terrestrial hydrological processes [*Yang et al*., 2011; *Cai et al*., 2014a, 2014b]. Because Noah-MP provides multiple schemes for selected processes, it is ideal for performing ensemble simulations.

Two experiments were performed in a multiple-parameterization ensemble approach using the FAO and BNU soil datasets and named after them. An ensemble of 12 Noah-MP members was configured with 4 runoff parameterization schemes and 3 $\beta$-factor schemes (Table 1). The runoff and $\beta$-factor schemes were selected as they dominate the modeling of soil moisture and its relationship with evapotranspiration [*Yang et al*., 2011]. The four runoff options are Simple Water Balance (SWB), Biosphere-Atmosphere Transfer Scheme (BATS), SIMple TOPMODEL (SIMTOP), and SIMple Groundwater Model (SIMGM). SWB, adopted by Noah [*Chen and Dudhia*, 2001], defines surface runoff as the component of total precipitation not infiltrated into the soil. BATS [*Dickinson et al*., 1993] employs the concept of "fractional saturated area" and models runoff as a function of surface soil moisture. SIMTOP [*Niu et al*., 2005] and SIMGM [*Niu et al*., 2007], based on TOPMODEL, take into

**Table 1.** Twelve Noah-MP Configurations and Their Parameterization Schemes

| Name | Runoff Scheme | $\beta$-Factor Scheme |
|---|---|---|
| A1 | SIMGM | Noah |
| A2 | SIMGM | CLM |
| A3 | SIMGM | SSiB |
| B1 | SIMTOP | Noah |
| B2 | SIMTOP | CLM |
| B3 | SIMTOP | SSiB |
| C1 | SWB | Noah |
| C2 | SWB | CLM |
| C3 | SWB | SSiB |
| D1 | BATS | Noah |
| D2 | BATS | CLM |
| D3 | BATS | SSiB |

account topographic effects and model runoff as a function of topography and water table depth. The first two have gravitational drainage boundary conditions, while the latter two have the water table as the lower boundary. The three $\beta$-factor options used in this paper are Noah-type (using soil moisture) [*Chen and Dudhia*, 2001], Community Land Model- (CLM-) type (using capillary potential) [*Oleson et al*., 2004], and Simplified Simple Biosphere- (SSiB-) type (also using capillary potential but expressed by a different function [*Xue et al*., 1991]). *Niu et al*. [2011] provided a detailed comparison of these three $\beta$-factor options.

All of the simulations were conducted at a spatial resolution of 0.25° in China using the atmospheric forcing and vegetation parameters from Global Land Data Assimilation System (GLDAS) [*Rodell et al*., 2004]. The GLDAS atmospheric forcing is based on the Princeton Global Meteorological Forcing Dataset of *Sheffield et al*. [2006], which was constructed from the combination of the National Centers for Environmental Prediction–National Center for Atmospheric Research (NCEP-NCAR) reanalysis and observation-corrected precipitation, air temperature, and radiation, taking into consideration of the changes of meteorological variables in elevation. The GLDAS datasets of land cover class [*Hansen et al*., 2000], leaf area index [*Gottschalck et al*., 2002], and green vegetation fraction [*Liang et al*., 2010] were all produced using observations obtained by the advanced very high resolution radiometer (AVHRR) satellites.

### 2.3. Model Spin-Up and Outputs

The spin-up was performed with a two-stage procedure for each experiment: (1) iteratively simulate the entire year of 1990 60 times (60 years) and (2) simulate another 12 year period from 1 January 1991 to 1 January 2003. Following the spin-up procedure, all experiments simulated the period from January 2003 to December 2012. The climatology, monthly means, and extreme daily values of the model results in this 10 year period were calculated and analyzed in this paper.

All model outputs (e.g., soil moisture, evapotranspiration, and runoff) were averaged across 12 ensemble members for each experiment to produce ensemble means. Because noticeable differences exist between the parameterization schemes, the ensemble means should average out the variation produced by individual members and provide more accurate estimates of hydrological variables [*Guo et al*., 2007; *Gudmundsson et al*., 2012; *Liu and Xie*, 2013].

Evapotranspiration (ET) ratio, runoff ratio, surface flow index (SFI), and normalized annual maximum flow (NAMF) were derived from the model outputs to measure surface water balances and floods. The ET ratio and runoff ratio measure the partitioning of precipitation between evapotranspiration and runoff. The ET ratio is defined as the ratio of annual mean evapotranspiration to the annual mean precipitation. The runoff ratio is defined as the ratio of annual mean total runoff to the annual mean precipitation. These two ratios are negatively related, and their sum equals 1 as a result of surface water balance [*Yang et al*., 2011]. The SFI measures the partitioning of annual mean total runoff between surface and subsurface components, and the NAMF represents the flood magnitude. The SFI is defined as the ratio of the annual surface runoff amount (mm) divided by the annual total runoff amount (mm) following *Guo et al*. [2014]. The NAMF is expressed as the mean maximum daily runoff (mm) divided by the annual mean runoff (mm) [*Vogel and Wilson*, 1996]. A large NAMF value indicates that relatively more runoff is generated in flood events. Although these two measures are different in meanings, *Guo et al*. [2014] showed that there is a significantly positive relationship between these two measures.

### 2.4. GRACE Terrestrial Water Storage Anomaly

The GRACE twin satellites accurately measure the changes in distance and speed between them and retrieve the temporal change of the Earth's gravity field [*Tapley et al*., 2004]. As other mass changes are relatively small, GRACE satellites primarily detect the changes in terrestrial water storage (TWS). *Landerer and Swenson* [2012] created monthly 1° TWS anomaly (TWSA) dataset based on standard GRACE product in the form of spherical harmonic coefficients. We used the CSR RL5.0 release from the Center for Space Research at the University of Texas at Austin and linearly interpolate it to the GLDAS grid.

### 2.5. MODIS Evapotranspiration (ET)

The global ET product of *Mu et al*. [2011] was used to evaluate modeled evapotranspiration. The product is based on the observations from MODIS on board NASA's Terra and Aqua satellites and agrees well with flux tower observations regarding bias (the relative error is about 24.1%). We obtained the monthly version of the

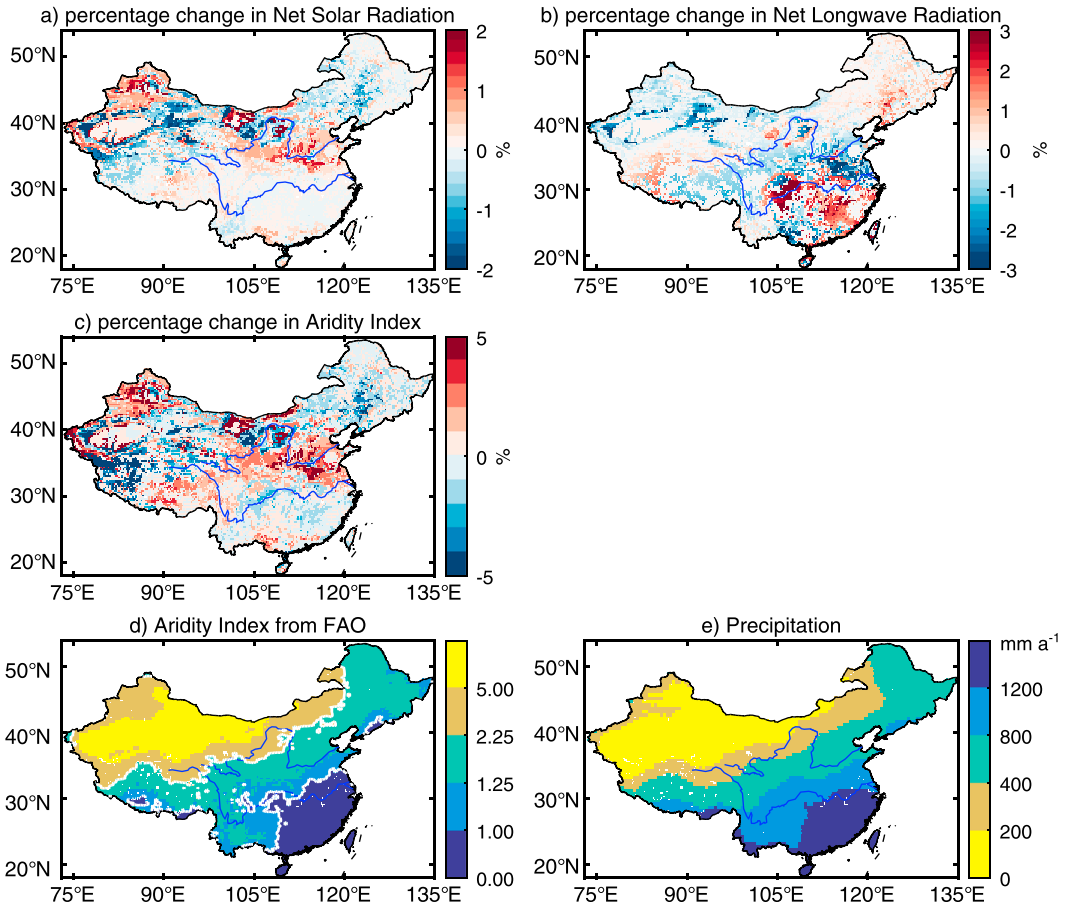


**Figure 2.** Geographic patterns of the percentage changes in (a) net solar radiation, (b) net longwave radiation, and (c) Budyko's aridity index from the FAO to the BNU experiment, (d) the aridity index from the FAO experiment, and (e) annual mean precipitation for the period of 2003 to 2012. The percentage change of a quantity is defined as the percentage of the change in the quantity between the two experiments to their arithmetic mean. The white lines (aridity index isopleths of 1.0 and 2.25) divide China into three areas: the humid zone, the transitional zone, and the arid zone.

product at 0.125° resolution and then derived the area-weighted annual means over the 0.25° GLDAS grid cells for the period of 2003 to 2012.

### 2.6. Budyko's Aridity Index

The aridity was measured by the Budyko's Aridity Index. It is defined as the ratio of annual potential evapotranspiration to annual precipitation, where annual potential evapotranspiration is expressed as the annual net radiation divided by the latent heat of vaporization for water [*Gerrits et al*., 2009]. In humid regions, the aridity index is less than 1, meaning that the annual net radiation is not sufficient to evaporate the annual precipitation. In arid regions, the aridity index is significantly larger than 1, the net radiation exceeds the required energy for the annual precipitation to evaporate, and actual evaporation is much smaller than potential evaporation. Depending on the aridity index, actual evaporation is limited by either net radiation or precipitation.

In this study, the aridity index was calculated using the ensemble mean of modeled net radiation for each of the two experiments. Figures 2a and 2b represent the differences in modeled surface radiation budgets from the FAO and BNU experiments. Similar to *Wilson et al*. [1987], the modeled net solar and longwave radiation have a very small response (the relative change is less than 5%) to the soil-type change. As a result, the aridity indices from the two experiments are well matched (Figure 2c).

Figure 2d shows the geographic distribution of the aridity index from the FAO experiment. The spatial pattern is consistent with the result from an empirical model by *Wu et al*. [2006], with the aridity index increasing from approximately 0.5 in the southeast to approximately 15 in the northwest. The aridity index

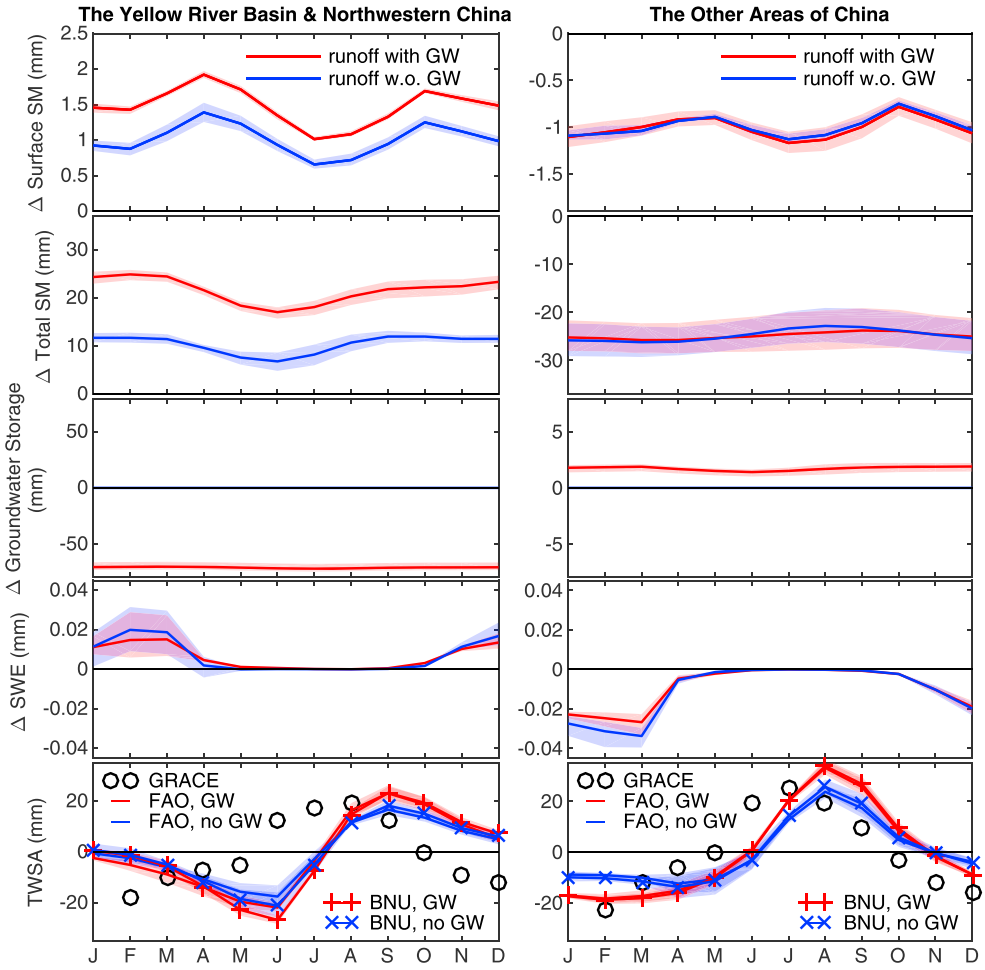


**Figure 3.** The changes in terrestrial water storage components from the FAO to the BNU experiment in two subregions (as defined in Figure 1b) of China. The red lines represent the ensemble means of members with groundwater (GW), and the blue lines represents those without groundwater. The black circles represent the observations from the GRACE satellites.

is closely related to the annual mean precipitation (Figure 2e). The 1 and 2.25 aridity index contours are close to the 1200 mm and 400 mm annual precipitation contours, respectively. Based on these contours, China is divided into three climatic regions: the humid region where the aridity index is less than 1, the arid region where the aridity index is greater than 2.25, and the transitional region between them.

It should be noted that the output in regions where daily evapotranspiration is less than 0.1 mm was discarded because a substantial uncertainty exists in the simulations over these extreme arid regions.

## 3. Results

### 3.1. Terrestrial Water Storage (TWS) and Its Anomaly (TWSA)

The TWS is the total water amount stored in soil, groundwater, and snow/ice, and the TWSA reflects the departure of the TWS from its climatology. We calculated the TWS from storage terms that include three variables (soil moisture, snow water equivalent, and groundwater storage) for runs with SIMGM and SIMTOP runoff options. For runs with SWB and BATS runoff options, which do not have a groundwater model, we calculated the TWS as the sum of two variables, soil moisture, and snow water equivalent only.

$$\mathrm{TWS}_i = \begin{cases} \mathrm{SMC}_i + \mathrm{SWE}_i + \mathrm{GW}_i & \text{for SIMGM and SIMTOP} \\ \mathrm{SMC}_i + \mathrm{SWE}_i & \text{for SWB and BATS} \end{cases} \quad (1)$$

where $\mathrm{SMC}_i$, $\mathrm{SWE}_i$, and $\mathrm{GW}_i$ are the total column (2 m) soil moisture storage, snow water equivalent, and groundwater storage, respectively.

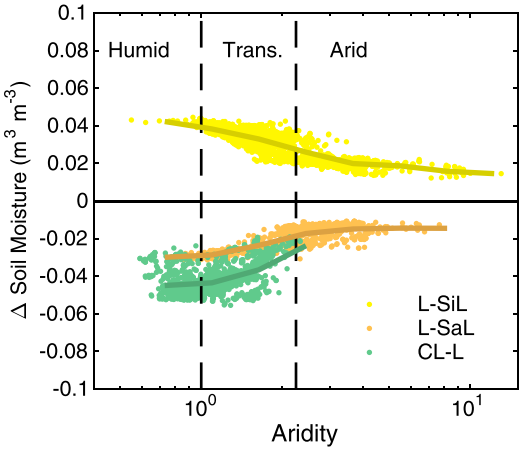


**Figure 4.** Influence of soil-type change on modeled surface soil moisture climatology (2003–2012) under different climatic conditions. L-SiL for the soil-type change from loam to silt loam, L-Sal for loam to sandy loam, and CL-L for clay loam to loam.

The differences in the modeled terrestrial water storage and its components between the FAO and BNU experiments are shown in Figure 3. The soil moisture in the Yellow River basin and northwest China is reduced as soil has more sand content; while in the other areas where soil has less sand content, the modeled soil moisture increases. The percentage change of the surface and total column soil moisture climatology in the two subregions are all around 5%. However, the seasonality of the terrestrial water storage has a small response to the soil dataset; thus, the modeled TWSA from the BNU experiment is close to that from the FAO experiment.

As shown in Figure 3, the sensitivity of modeled terrestrial water storage differs with parameterization schemes, depending on the existence of a groundwater model. Ensemble members with a groundwater model are more sensitive (measured by the difference between the two experiments) than those without a groundwater model. Comparing the ensemble means from the FAO (BNU) experiment with the GRACE observations, the correlation coefficients of modeled monthly TWSA from the groundwater-included members are 0.356 and 0.557 (0.362 and 0.556) in the two subregions and the corresponding values are 0.330 and 0.491 (0.320 and 0.506) for those members without groundwater.

### 3.2. Soil Moisture Climatology

Similar to previous studies [*Xia et al*., 2015], the modeled soil moisture climatology is found strongly depending on soil type. As shown in Figure 4, the relative changes in soil moisture are +12%, −8.5%, and −13% when the soil type is changed from loam to silty loam, from loam to sandy loam, and from clay loam to loam, respectively. These values are close to the corresponding changes in field capacity, which are +0.04, −0.02, and $-0.05\,m^3\,m^{-3}$. Figure 4 also illustrates how these soil moisture changes vary with the aridity index. The maximum difference in soil moisture between the FAO and BNU experiments appears in humid regions (where the aridity index is less than 1). With increasing aridity, the soil tends to dry completely regardless of soil type, so the difference in soil moisture between the FAO and BNU experiments approaches zero.

The dependency of soil moisture to soil type can be expressed quantitatively as the sensitivity to soil's sand and clay content; we find that the sand content largely controls the soil moisture in the simulations. Figure 5 shows the relationships between soil moisture and soil texture, and their statistics are given in Table 2. As the soil gets sandier, it has smaller pore spaces and lower field capacity [*Chen and Dudhia*, 2001], and models produce drier mean soil conditions. The sensitivity to sand content (expressed as the slope of the linear regression between soil moisture and sand content) varies with aridity. In arid regions, the sensitivity to sand content (shown in Figure 5) is $-0.80\times10^{-3}\,m^3\,m^{-3}$ per sand%, the same as the value estimated from satellite observations at an arid site in central Tunisia by *Gorrab et al*. [2015]. The sensitivity increases as the environment gets wetter. In humid regions, the soil moisture sensitivity to sand content is approximately tripled to $-2.2\times10^{-3}\,m^3\,m^{-3}$ per sand%.

The geographic distribution of soil moisture change is shown in Figure 6a. Comparing it with the sand content difference in Figure 1b, the soil moisture change is inversely proportional to the sand content change. In

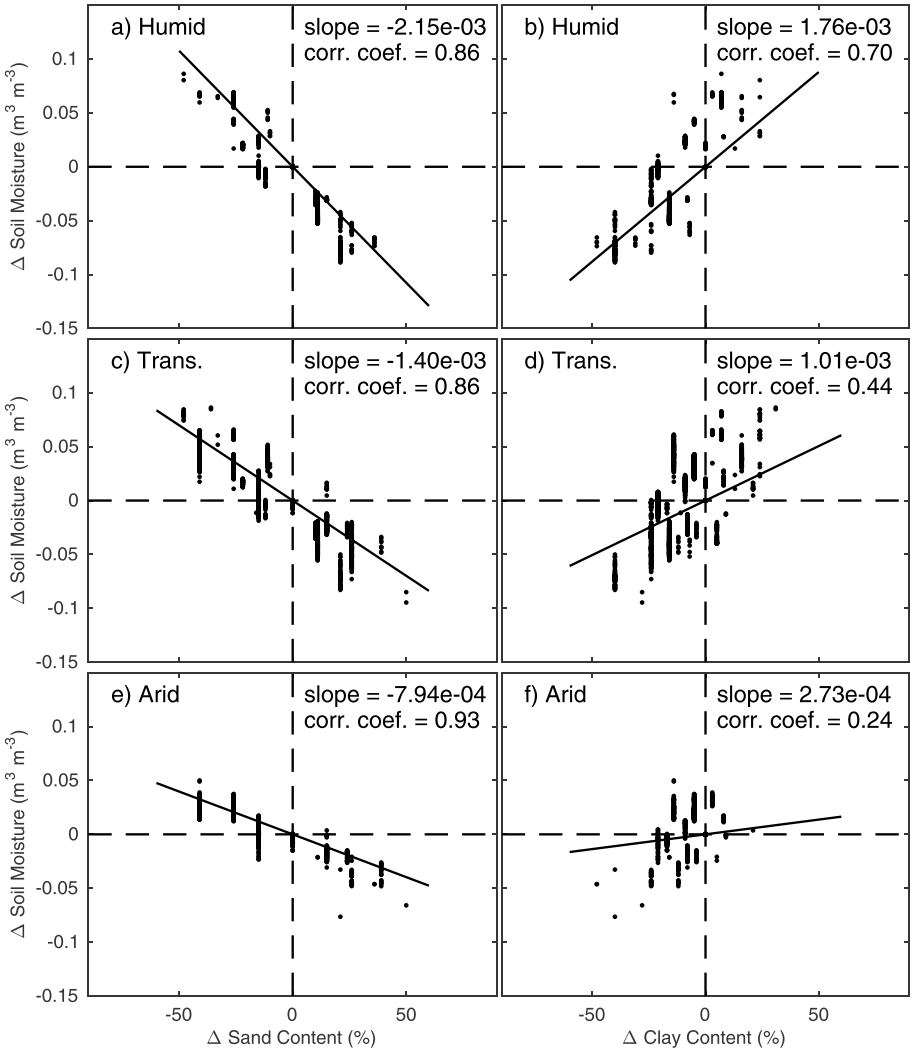


**Figure 5.** (a–f) Relationships between soil moisture changes from the FAO experiment to the BNU experiment and corresponding soil texture differences in different climatic regions. The solid lines represent the linear regression lines. The slope of the linear regression line and the correlation coefficient are shown in each plot.

the Yellow River basin where the soil has less sand, the simulated soil moisture from the BNU experiment is higher than that from the FAO experiment, while elsewhere with sandier soil, the BNU experiment yield lower soil moisture estimates.

The geographic pattern of the soil moisture sensitivity to sand content is shown in Figure 6b. By comparing it with the aridity index distribution in Figure 2, it is clear that the spatial pattern of the sensitivity is governed by the climatic regime. It is most sensitive in humid regions, and sensitivity decreases with increasing aridity from southeast to northwest.

### 3.3. Partitioning Between Evapotranspiration and Runoff

*Seneviratne et al.* [2010] conceptually summarized the distinct roles of soil moisture in controlling evapotranspiration in the three climate regions. In humid regions, net radiation limits evapotranspiration, and the evaporative fraction of precipitation is independent of soil moisture. In arid regions, if soil moisture is below wilting point, no evapotranspiration will take place regardless of the moisture variations. In the transitional regions, soil moisture is the most important constraint on evapotranspiration.

Figure 7a represents the differences in modeled evapotranspiration between the two experiments. The geographic pattern is similar to the soil moisture shown in Figure 6a. In the Yellow River basin where the soil is

**Table 2.** Sensitivities of Simulated Terrestrial Water Variables to the Sand and Clay Content Across 12 Parameterization Schemes and 3 Climatic Regions (Humid, Transitional, and Arid Regions)[a]

| | | Surface Soil Moisture ($\times 10^{-3}$ $m^3/m^3/\%$) | | | Evapotranspiration Ratio ($\times 10^{-3}$ mm/mm/%) | | | Surface Flow Index ($\times 10^{-3}$ mm/mm/%) | | | Normalized Maximum Flood Index ($\times 10^{-3}$ mm/mm/%) | | |
|---|---|---|---|---|---|---|---|---|---|---|---|---|---|
| Model | Soil | Humid | Transitional | Arid | Humid | Transitional | Arid | Humid | Transitional | Arid | Humid | Transitional | Arid |
| A1 | Sand | −2.40 | −1.63 | −0.75 | −2.73 | −3.92 | −2.66 | −0.56 | - | −13.4 | - | - | −3.84 |
| | Clay | 1.98 | - | - | - | - | - | - | - | - | - | - | - |
| A2 | Sand | −2.40 | −1.64 | −0.90 | −2.66 | −3.63 | −2.37 | −0.55 | - | −13.5 | - | - | −4.01 |
| | Clay | 1.98 | - | - | - | - | - | - | - | - | - | - | - |
| A3 | Sand | −2.40 | −1.63 | −0.86 | −2.67 | −3.63 | −2.38 | −0.55 | - | −13.3 | - | - | −3.88 |
| | Clay | 1.98 | - | - | - | - | - | - | - | - | - | - | - |
| B1 | Sand | −2.32 | −1.58 | −0.85 | −2.21 | −3.56 | −3.50 | −0.89 | −2.64 | −7.97 | −0.28 | −0.33 | −1.08 |
| | Clay | 1.66 | - | - | - | - | - | - | - | - | - | - | - |
| B2 | Sand | −2.32 | −1.60 | −1.00 | −2.18 | −3.35 | −3.19 | −0.89 | −2.61 | −7.50 | −0.28 | −0.33 | −0.99 |
| | Clay | 1.66 | - | - | - | - | - | - | - | - | - | - | - |
| B3 | Sand | −2.32 | −1.59 | −0.96 | −2.19 | −3.35 | −3.16 | −0.89 | −2.67 | −7.68 | −0.28 | −0.33 | −1.02 |
| | Clay | 1.66 | - | - | - | - | - | - | - | - | - | - | - |
| C1 | Sand | −2.13 | −1.26 | −0.59 | −1.80 | −1.98 | −1.26 | −8.66 | −5.84 | - | −0.69 | - | - |
| | Clay | 1.73 | - | - | - | - | - | 11.1 | 9.77 | - | 0.83 | - | - |
| C2 | Sand | −2.13 | −1.28 | −0.76 | −1.77 | −1.81 | - | −8.66 | −5.63 | - | −0.69 | - | - |
| | Clay | 1.73 | - | - | - | - | - | 11.1 | 9.47 | - | 0.83 | - | - |
| C3 | Sand | −2.13 | −1.26 | −0.73 | −1.78 | −1.85 | - | −8.66 | −5.72 | - | −0.69 | - | - |
| | Clay | 1.73 | - | - | - | - | - | 11.2 | 9.44 | - | 0.83 | - | - |
| D1 | Sand | −1.76 | −1.09 | −0.61 | −1.52 | −1.49 | −1.39 | −7.58 | - | −4.11 | −0.34 | - | - |
| | Clay | 1.66 | - | - | - | - | - | 11.4 | 13.4 | - | 0.53 | 1.06 | - |
| D2 | Sand | −1.76 | −1.11 | −0.77 | −1.46 | −1.23 | - | −7.58 | - | - | −0.34 | - | - |
| | Clay | 1.67 | - | - | - | - | - | 11.4 | 13.2 | - | 0.52 | 1.03 | - |
| D3 | Sand | −1.76 | −1.09 | −0.74 | −1.48 | −1.30 | - | −7.59 | - | - | −0.34 | - | - |
| | Clay | 1.66 | - | - | - | - | - | 11.4 | 13.2 | - | 0.53 | 1.02 | - |
| Mean | Sand | −2.15 | −1.40 | −0.79 | −2.04 | −2.59 | −1.99 | −4.42 | −4.11 | −6.99 | −0.36 | −0.48 | −1.52 |
| | Clay | 1.76 | 1.01 | 0.27 | 1.08 | - | - | 5.86 | 5.35 | - | 0.42 | - | - |

[a]The sensitivity is defined as the slope of linear regression. "-" indicates that the corresponding coefficient determination is less than 0.4.

dryer, the simulated evapotranspiration from the BNU experiment is lower than that from the FAO experiment, while elsewhere with wetter soils, the BNU experiment yield higher evapotranspiration estimates. Table 3 compares the estimates from the two experiments with the MODIS observations. In the Yellow River basin and northwest China, the BNU experiment outperforms the FAO experiment.

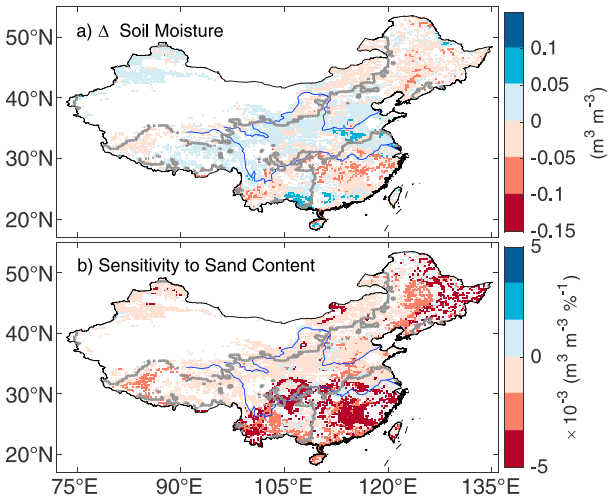


**Figure 6.** Spatial pattern of (a) soil moisture changes and (b) their sensitivity to sand content changes. The deeper colors in Figure 6b indicate larger sensitivities. The gray lines are the 1.0 and 2.25 aridity index contours.

Figure 7b shows the sensitivity of modeled evapotranspiration to soil moisture. We define this sensitivity as the ratio of the change in the evapotranspiration ratio to the change in soil moisture climatology. As expected from the above conceptual model, the results show that evapotranspiration is most sensitive to soil moisture in the transitional regions, where soil moisture is also strongly correlated with precipitation [*Koster et al.*, 2004].

The sensitivity of evapotranspiration to soil type is a product of two components linked by soil moisture: the sensitivity of evapotranspiration to soil moisture (Figure 8a) and the sensitivity of soil moisture to soil type (Figure 4). Figure 8b shows the sensitivity of evapotranspiration to soil-type change at different levels of aridity, and Table 2 summarizes the coefficients of these

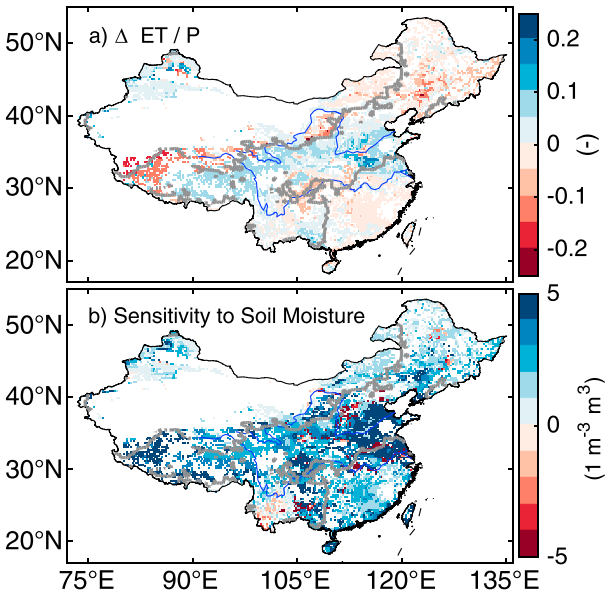


**Figure 7.** Geographic distribution of differences in (a) evapotranspiration ratio (defined as the ratio of annual mean evapotranspiration to the annual mean precipitation) and (b) its sensitivities to surface soil moisture changes. The sensitivity is defined as the ratio of the changes in the evapotranspiration ratio to the changes in the surface soil moisture climatology (averaged from 2003 to 2012). The gray lines are the 1.0 and 2.25 aridity index contours.

relationships. The relatively low values in both humid and arid regions suggest that the annual mean evapotranspiration is weakly dependent on soil moisture climatology in these regions. The maximum sensitivity occurs in the transitional zones, indicating a significant effect of soil type on evapotranspiration there.

The precipitation that does not evaporate generates runoff. The sensitivity of runoff to soil type (Figure 8 c) is negatively proportional to that of evapotranspiration. As in the case of evapotranspiration, runoff is most sensitive to soil-type changes in the transitional regions.

### 3.4. Partitioning Between Surface and Subsurface Runoff and Flood Indices

Soil-type changes can substantially alter the partitioning of the runoff between the fast component (surface runoff) and the slow component (subsurface runoff) [*Osborne et al*., 2004]. Figure 9a shows the geographic distribution of SFI changes between the two experiments. Relative to the FAO experiment, the BNU experiment produces a smaller surface flow fraction in southern and northeastern China. In these regions, the BNU soil data have more sand than the FAO data (Figure 1b). The sandier soil has a larger infiltration capacity; thus, surface flow is reduced [*Mein and Larson*, 1973]. In the Yellow River basin and northwestern China, where soils have more clay and less sand, the results using the BNU data produce about one fifth more surface flow than the results using the FAO dataset. This negative relationship between SFI and sand content is given in Table 2.

The changes in annual mean water balance could influence the flood statistics [*Livneh et al*., 2015]. Figure 9b shows the geographic pattern of the NAMF change. By comparing it with Figure 9a, it is clear that the change in the NAMF values are closely related to the SFI. In northwestern China and the Yellow River basin where the SFI is higher, the flood magnitude (indicated by the NAMF values) also increases, a result that is consistent with *Guo et al*. [2014]. A higher SFI implies an impermeable underlying surface, leading to a reduction of water storage in the soil layer during peak precipitation.

While soil type influences the SFI and NAMF by changing surface permeability, the influence is greater in arid regions than in humid regions as more bare soil exists under a dry climate. Figure 10 shows the dependencies of the SFI and NAMF on the aridity indices for the three soil-type changes. Using L-SiL as an example, the surface flow index difference between the FAO and BNU experiments increases from approximately 0 in humid regions to approximately 0.3 in arid regions. At the same time, the change in NAMF increases from 0 in humid regions to near 0.1 in arid regions, indicating that the BNU experiment, on average, gathers approximately 10% more the annual runoff in one single flood event than the FAO experiment.

### 3.5. The Sensitivity Consistency Across Different Parameterization Schemes

For the soil-type change of loam to silt loam, Figure 11 compares the differences in water balance components from different ensemble members. Table 2 summarizes the model sensitivity to soil texture for each ensemble member. The relationship of model sensitivity to the aridity is similar across parameterization schemes, of which the patterns were analyzed in previous sections using the ensemble means. The ensemble

**Table 3.** Comparisons of Estimated Annual Mean Evapotranspiration for Different Parameterization Schemes and Soil Datasets with MODIS Observations[a]

| | The Yellow River Basin and the Northwest China | | The Other Areas of China | |
|---|---|---|---|---|
| Model | FAO | BNU | FAO | BNU |
| A1 | 408 | 433 | 529 | 520 |
| A2 | 412 | 436 | 533 | 525 |
| A3 | 413 | 436 | 535 | 526 |
| B1 | 413 | 436 | 545 | 538 |
| B2 | 416 | 438 | 547 | 542 |
| B3 | 417 | 439 | 549 | 544 |
| C1 | 419 | 429 | 437 | 430 |
| C2 | 421 | 432 | 540 | 534 |
| C3 | 422 | 432 | 541 | 536 |
| D1 | 378 | 385 | 498 | 488 |
| D2 | 383 | 390 | 503 | 495 |
| D3 | 385 | 392 | 505 | 498 |
| AB | 413 | 436 | 540 | 532 |
| CD | 401 | 410 | 521 | 514 |
| ALL | 407 | 423 | 530 | 523 |
| MODIS | 463 | | 580 | |

[a]AB represents the arithmetic ensemble means of the parameterization schemes with groundwater, and CB represents those without groundwater.

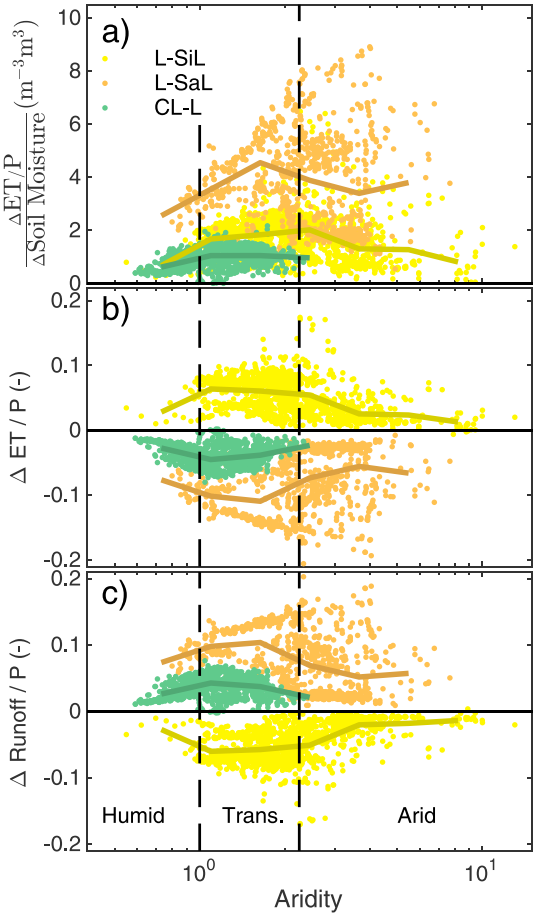


**Figure 8.** Same as in Figure 4 but for (a) the sensitivity of evapotranspiration ratio to soil moisture, (b) the change in evapotranspiration ratio, and (c) runoff ratio.

members with a groundwater model are more sensitive to the soil-type change, especially for the partitioning of surface and subsurface runoff (SFI) and flood indexes (NAMF).

The differences for the soil moisture and evapotranspiration ratio are largely due to how groundwater recharge is modeled. The SIMTOP and SIMGM runoff schemes model groundwater recharge as a production of soil hydraulic conductivity and the difference of water tension between the soil bottom and the water table [*Niu et al.*, 2005, 2007], while the free drainage schemes (NOAH and BATS) do not take the water tension into consideration [*Chen and Dudhia*, 2001; *Dickinson et al.*, 1993]. As a result, changing soil type from loam to silt loam (Figure 11), the groundwater recharge rate decreases less in NOAH and BATS than in SIMTOP and SIMGM. Consequently, soil moisture and the evapotranspiration ratio increase less in these schemes without groundwater.

The differences of the sensitivity in SFI and NAMF are larger than in soil moisture and evapotranspiration ratio, reflecting the difference of how subsurface runoff is modeled. The NOAH and BATS runoff schemes treat the subsurface runoff the same as the groundwater recharge [*Chen and Dudhia*,

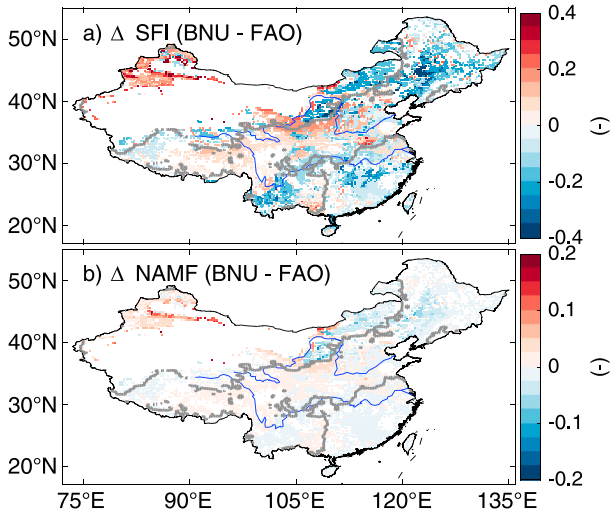


**Figure 9.** Geographic distribution of changes of flood indexes from FAO to BNU, (a) surface flow index (SFI), and (b) normalized annual maximum flood (NAMF), respectively. The gray lines are the 1.0 and 2.25 aridity index contours.

2001; *Dickinson et al.*, 1993], while the SIMTOP and SIMGM model it as a function of groundwater table depth [*Niu et al.*, 2005, 2007]. Reflecting the change in the water table depth (Figure 11), modeled subsurface reduces more in SIMGM and SIMTOP, resulting in higher SFI and NAMF values.

## 4. Discussion

As complex interactions exist between atmospheric forcing, physical processes, and various parameters [*Rosero et al.*, 2010], several factors may influence the generality of our work. First, the Noah-MP ensemble was constructed from different parameterization schemes for runoff and $\beta$-factor, which are the two most important processes reported by previous studies [*Yang et al.*, 2011]. Obviously, this ensemble does not reflect all parameterization schemes available in the modeling community. It is possible that including new schemes into Noah-MP may result in more generalizable results. Second, as precipitation is one of the most important constraints on hydrological simulations [*Wang and Zeng*, 2011], different precipitation datasets may result in different estimates of the magnitude of soil-type effects [*Liu and Xie*, 2013]. However, as Budyko's aridity index has already taken the precipitation into account, the relationships between the soil-type sensitivity and the aridity index are unlikely to change.

Many authors argued that vegetation has a significant impact on modeled evapotranspiration at plot scales [*Zhang et al.*, 2001; *Gulden et al.*, 2008; *Xia et al.*, 2015]. We found that the vegetation type can affect the magnitude of the model sensitivity, but the pattern of how the model sensitivity varies with aridity will not change. Figure 12 represents the model sensitivities to the soil-type change of loam to silt loam under two different vegetation types. The difference between the two vegetation types is most significant in the modeling of evapotranspiration and is negligible for the soil moisture. The change of evapotranspiration ratio is reduced by 47% under the denser vegetation type (mixed forest relative to grassland). Regardless of the

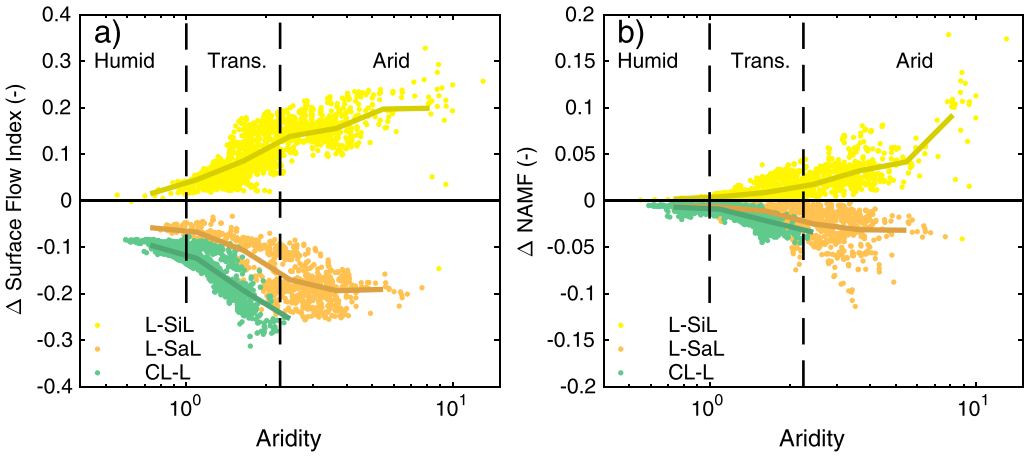


**Figure 10.** Same as in Figure 4 but for (a) surface flow index (surface runoff divided by total runoff) and (b) normalized annual maximum flood (NAMF).

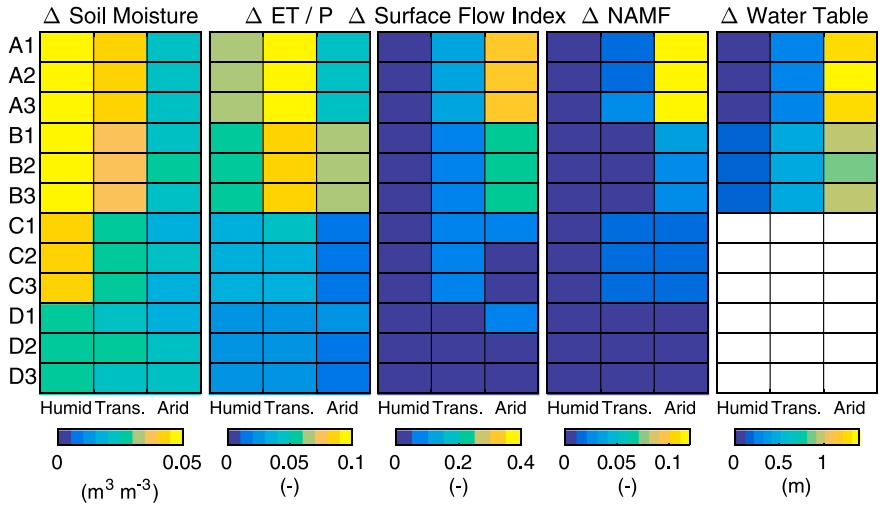


**Figure 11.** Comparisons of changes in soil moisture, evapotranspiration ratio, surface flow index, normalized annual maximum flow, and water table from loam to silt loam for the 12 ensemble members.

vegetation type, the difference of the modeled evapotranspiration ratio peaks in the transitional zones, showing that the controlling effects of the aridity on the model sensitivity should be robust.

Our findings suggest that soil-type datasets have profound implications for climate predictability in the transitional regions. The results show that the simulated evapotranspiration is most sensitive to soil texture type in the

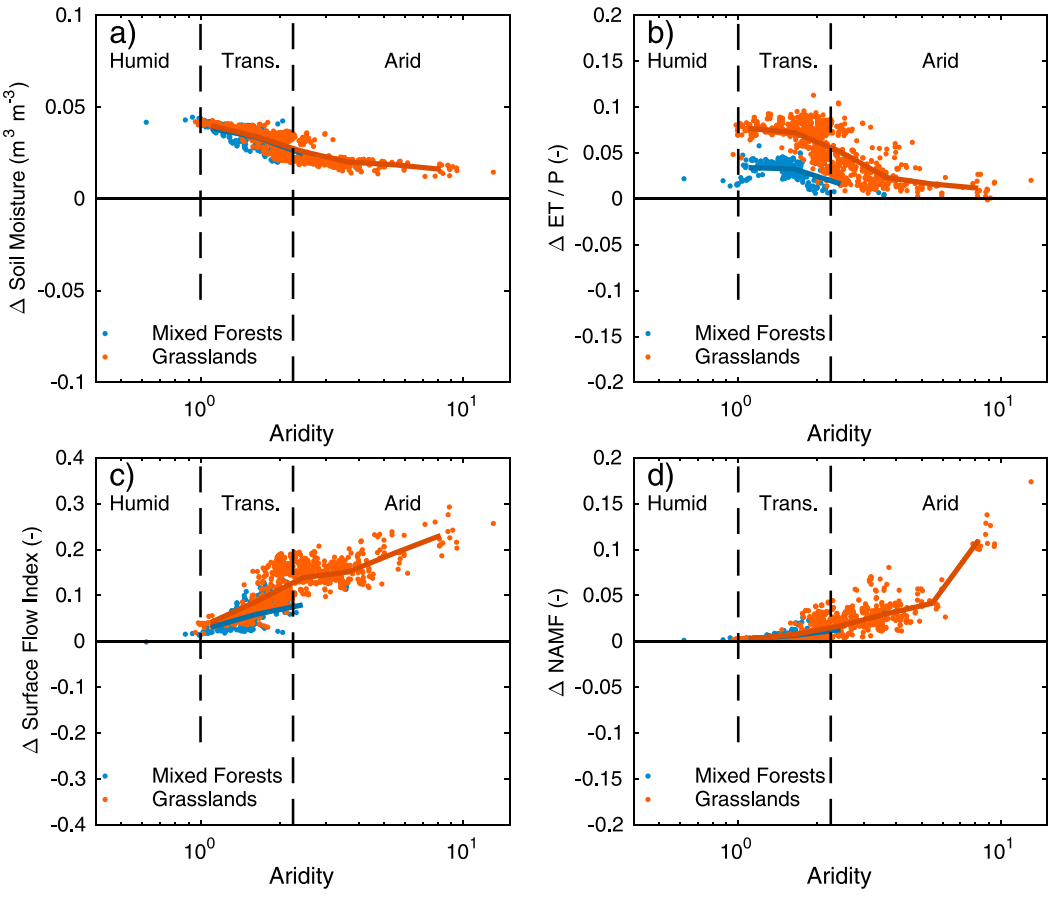


**Figure 12.** Comparisons of the changes in (a) soil moisture, (b) evapotranspiration ratio, (c) surface flow index, and (d) normalized annual maximum flow for the soil-type change from loam to silt loam under two different vegetation cover types.

transitional regions, which are also the hot spots of land-atmosphere coupling strength [*Koster et al*., 2004]. Sandier soil types in these regions may reduce the land-atmosphere coupling strength by reducing both the amount of water stored in soil (soil moisture) and the water exchange between the land and the atmosphere (evapotranspiration). Consequently, the predictability of the coupled land-atmosphere model would be reduced if the sand content is increased in the soil-type dataset. Still, this hypothesis remains to be tested.

## 5. Conclusions

This study assessed soil-type-induced changes in hydrological simulations under different climatic conditions by employing the state-of-art Noah-MP LSM and a multiple-parameterization ensemble approach.

Geographic comparisons of the two simulations based on the FAO and BNU soil datasets show that the selected hydrological variables are very sensitive to soil-type descriptions. The most frequent soil-type change from the FAO dataset to the BNU dataset is from loam to silt loam, which covers 16% of the land area in China, mostly in the semiarid and semihumid regions. As a result, modeled soil moisture increases by 12%, the ratio of evapotranspiration to precipitation increases by 6%, the fraction of surface runoff to total runoff increases by 25%, and the normalized annual maximum flood increases by 28%.

We analyzed the model sensitivity under different climate conditions. We found that aridity is a first-order factor in regulating the model sensitivity and that the selected hydrologic variables respond to the climate in different ways. For soil moisture, the influence of soil type decreases with increasing aridity. For the partitioning of precipitation between evapotranspiration and runoff, soil type has the largest effect in the climatological transition zones. For flood magnitude, its sensitivity to soil type increases with the aridity index.

We also analyzed the consistency of model sensitivity across different parameterization schemes and found that the model sensitivities to soil type are mainly dominated by runoff schemes. Schemes with a groundwater model show greater sensitivity to soil-type changes.

**Acknowledgments**

This work is supported by the National Natural Science Foundation of China grant 41375088. The authors would like to thank Zhongfeng Xu for the assistance in preparing the figures. The atmospheric forcing and vegetation parameter datasets can be downloaded from the GLDAS website (http://ldas.gsfc.nasa.gov/gldas). The soil dataset developed by *Shangguan et al*. [2012] can be obtained from Beijing Normal University (http://globalchange.bnu.edu.cn/research/soil). GRACE terrestrial water storage data can be downloaded from Jet Propulsion Laboratory TELLUS website (http://grace.jpl.nasa.gov). MODIS evapotranspiration data are from *Mu et al*. [2011] (http://www.ntsg.umt.edu/project/mod16). The model output data presented here are available upon request from the author (zhenghui@tea.ac.cn).

## References

Arora, V. K. (2002), The use of the aridity index to assess climate change effect on annual runoff, *J. Hydrol.*, *265*(1–4), 164–177, doi:10.1016/S0022-1694(02)00101-4.

Bastidas, L. A., T. S. Hogue, S. Sorooshian, H. V. Gupta, and W. J. Shuttleworth (2006), Parameter sensitivity analysis for different complexity land surface models using multicriteria methods, *J. Geophys. Res.*, *111*, D20101, doi:10.1029/2005JD006377.

Cai, X., Z.-L. Yang, C. H. David, G.-Y. Niu, and M. Rodell (2014a), Hydrological evaluation of the Noah-MP land surface model for the Mississippi River basin, *J. Geophys. Res. Atmos.*, *119*, 23–38, doi:10.1002/2013JD020792.

Cai, X., Z.-L. Yang, Y. Xia, M. Huang, H. Wei, L. R. Leung, and M. B. Ek (2014b), Assessment of simulated water balance from Noah, Noah-MP, CLM, and VIC over CONUS using the NLDAS test bed, *J. Geophys. Res. Atmos.*, *119*, 13,751–13,770, doi:10.1002/2014JD022113.

Chen, F., and J. Dudhia (2001), Coupling an advanced land surface hydrology model with the Penn State NCAR MM5 modeling system. Part I: Model implementation and sensitivity, *Mon. Weather Rev.*, *129*(4), 569–585, doi:10.1175/1520-0493(2001)129<0569:CAALSH>2.0.CO;2.

Cosby, B. J., G. M. Hornberger, R. B. Clapp, and T. R. Ginn (1984), A statistical exploration of the relationships of soil moisture characteristics to the physical properties of soils, *Water Resour. Res.*, *20*, 682–690, doi:10.1029/WR020i006p00682.

De Lannoy, G. J. M., R. D. Koster, R. H. Reichle, S. P. P. Mahanama, and Q. Liu (2014), An updated treatment of soil texture and associate hydraulic properties in a global land modeling system, *J. Adv. Model. Earth Syst.*, *6*(4), 957–979, doi:10.1002/2014MS000330.

Dickinson, R. E., A. Henderson-Sellers, and P. J. Kennedy (1993), Biosphere–Atmosphere Transfer Scheme (BATS) version 1e as coupled to the NCAR Community Climate Model, *NCAR Tech. Note TN383+STR*, NCAR.

FAO/UNESCO (1971–1981), *The FAO-UNESCO Soil Map of the World. Legend and 9 Volumes*, UNESCO, Paris.

Gao, Y., K. Li, F. Chen, Y. Jiang, and C. Lu (2015), Assessing and improving Noah-MP land model simulations for the central Tibetan Plateau, *J. Geophys. Res. Atmos.*, *120*, 9258–9278, doi:10.1002/2015JD023404.

Gerrits, A. M. J., H. H. G. Savenije, E. J. M. Veling, and L. Pfister (2009), Analytical derivation of the Budyko curve based on rainfall characteristics and a simple evaporation model, *Water Resour. Res.*, *45*, W04403, doi:10.1029/2008WR007308.

Gorrab, A., M. Zribi, N. Baghdadi, B. Mougenot, P. Fanise, and Z. L. Chabaane (2015), Retrieval of both soil moisture and texture using TerraSAR-X images, *Remote Sens.*, *7*(8), 10,098–10,116, doi:10.3390/rs70810098.

Gottschalck, J., P. Houser, and X. Zeng (2002), Impact of remotely sensed leaf area index on a global land data assimilation system, paper J1.15 presented at 16th Conference on Hydrology, Am. Meteorol. Soc., Orlando, Fla.

Gudmundsson, L., T. Wagener, L. M. Tallaksen, and K. Engeland (2012), Evaluation of nine large-scale hydrological models with respect to the seasonal runoff climatology in Europe, *Water Resour. Res.*, *48*, W11504, doi:10.1029/2011WR010911.

Gulden, L. E., Z.-L. Yang, and G.-Y. Niu (2008), Sensitivity of biogenic emissions simulated by a land-surface model to land-cover representations, *Atmos. Environ.*, *42*(18), 4185–4197, doi:10.1016/j.atmosenv.2008.01.045.

Guo, J., H.-Y. Li, L. R. Leung, S. Guo, P. Liu, and M. Sivapalan (2014), Links between flood frequency and annual water balance behaviors: A basis for similarity and regionalization, *Water Resour. Res.*, *50*, 937–953, doi:10.1002/2013WR014374.

Guo, Z., P. A. Dirmeyer, X. Gao, and M. Zhao (2007), Improving the quality of simulated soil moisture with a multi-model ensemble approach, *Q. J. R. Meteorol. Soc.*, *133*(624), 731–747.

Hansen, M. C., R. S. DeFries, J. R. G. Townshend, and R. Sohlberg (2000), Global land cover classification at 1 km spatial resolution using a classification tree approach, *Int. J. Remote Sens.*, *21*, 1331–1364, doi:10.1080/014311600210209.

Henderson-Sellers, A., Z.-L. Yang, and R. E. Dickinson (1993), The project for intercomparison of land-surface parameterization schemes, *Bull. Am. Meteorol. Soc.*, *74*(7), 1335–1349, doi:10.1175/1520-0477(1993)074<1335:TPFIOL>2.0.CO;2.

Hirabayashi, Y., R. Mahendran, S. Koirala, L. Konoshima, D. Yamazaki, S. Watanabe, H. Kim, and S. Kanae (2013), Global flood risk under climate change, *Nat. Clim. Change*, *3*(9), 816–821.

Koster, R. D., et al. (2004), Regions of strong coupling between soil moisture and precipitation, *Science*, *305*(5687), 1138–1140, doi:10.1126/science.1100217.

Landerer, F. W., and S. C. Swenson (2012), Accuracy of scaled GRACE terrestrial water storage estimates, *Water Resour. Res.*, *48*(4), W04531, doi:10.1029/2011WR011453.

Liang, L., F. N. Kogan, W. Guo, J. D. Tarpley, K. E. Mitchell, M. B. Ek, Y. Tian, W. Zheng, C.-Z. Zou, and B. H. Ramsay (2010), Real-time weekly global green vegetation fraction derived from advanced very high resolution radiometer-based NOAA operational global vegetation index (GVI) system, *J. Geophys. Res.*, *115*, D11114, doi:10.1029/2009JD013204.

Liu, G. (1999), Soil conservation and sustainable agriculture on the Loess Plateau: Challenges and prospects, *Ambio*, *28*(8), 663–668.

Liu, J.-G., and Z.-H. Xie (2013), Improving simulation of soil moisture in China using a multiple meteorological forcing ensemble approach, *Hydrol. Earth Syst. Sci.*, *17*, 3355–3369, doi:10.5194/hess-17-3355-2013.

Livneh, B., R. Kumar, and L. Samaniego (2015), Influence of soil textural properties on hydrologic fluxes in the Mississippi River basin, *Hydrol. Processes*, *29*(21), 4638–4655, doi:10.1002/hyp.10601.

Mein, R. G., and C. L. Larson (1973), Modeling infiltration during a steady rain, *Water Resour. Res.*, *9*, 384–394, doi:10.1029/WR009i002p00384.

Mu, Q., M. Zhao, and S. W. Running (2011), Improvements to a MODIS global terrestrial evapotranspiration algorithm, *Remote Sens. Environ.*, *115*(8), 1781–1800, doi:10.1016/j.rse.2011.02.019.

Niu, G.-Y., Z.-L. Yang, R. E. Dickinson, and L. E. Gulden (2005), A simple TOPMODEL-based runoff parameterization (SIMTOP) for use in global climate models, *J. Geophys. Res.*, *110*, D21106, doi:10.1029/2005JD006111.

Niu, G.-Y., Z.-L. Yang, R. E. Dickinson, L. E. Gulden, and H. Su (2007), Development of a simple groundwater model for use in climate models and evaluation with Gravity Recovery and Climate Experiment data, *J. Geophys. Res.*, *112*, D07103, doi:10.1029/2006JD007522.

Niu, G.-Y., et al. (2011), The community Noah land surface model with multiparameterization options (Noah-MP): 1. Model description and evaluation with local-scale measurements, *J. Geophys. Res.*, *116*, D12109, doi:10.1029/2010JD015139.

Oleson, K. W., et al. (2004), Technical description of the Community Land Model (CLM), *NCAR Tech. Note NCAR/TN-461+STR*, 174 pp., Natl. Cent. for Atmos. Res., Boulder, Colo. [Available at www.cgd.ucar.edu/tss/clm/distribution/clm3.0/index.html.]

Osborne, T. M., D. M. Lawrence, J. M. Slingo, A. J. Challinor, and T. R. Wheeler (2004), Influence of vegetation on the local climate and hydrology in the tropics: sensitivity to soil parameters, *Clim. Dyn.*, *23*(1), 45–61, doi:10.1007/s00382-004-0421-1.

Reynolds, C. A., T. J. Jackson, and W. J. Rawls (2000), Estimating soil water-holding capacities by linking the Food Agriculture Organization soil map of the world with global pedon databases, continuous pedotransfer functions, *Water Resour. Res.*, *36*, 3653–3662, doi:10.1029/2000WR900130.

Richter, H., A. W. Western, and F. H. S. Chiew (2004), The effect of soil and vegetation parameters in the ECMWF land surface scheme, *J. Hydrometeorol.*, *5*(6), 1131–1146, doi:10.1175/JHM-362.1.

Rodell, M., et al. (2004), The Global Land Data Assimilation System, *Bull. Am. Meteorol. Soc.*, *85*(3), 381–394, doi:10.1175/BAMS-85-3-381.

Rosero, E., Z.-L. Yang, T. Wagener, L. E. Gulden, S. Yatheendradas, and G.-Y. Niu (2010), Quantifying parameter sensitivity, interaction, and transferability in hydrologically enhanced versions of the Noah land surface model over transition zones during the warm season, *J. Geophys. Res.*, *115*, D03106, doi:10.1029/2009JD012035.

Rost, S., D. Gerten, A. Bondeau, W. Lucht, J. Rohwer, and S. Schaphoff (2008), Agricultural green and blue water consumption and its influence on the global water system, *Water Resour. Res.*, *44*, W09405, doi:10.1029/2007WR006331.

Seneviratne, S. I., T. Corti, E. L. Davin, M. Hirschi, E. B. Jaeger, I. Lehner, B. Orlowsky, and A. J. Teuling (2010), Investigating soil moisture–climate interactions in a changing climate: A review, *Earth Sci. Rev.*, *99*(3-4), 125–161, doi:10.1016/j.earscirev.2010.02.004.

Shangguan, W., Y. Dai, B. Liu, A. Ye, and H. Yuan (2012), A soil particle-size distribution dataset for regional land and climate modelling in China, *Geoderma*, *171–172*, 85–91, doi:10.1016/j.geoderma.2011.01.013.

Sheffield, J., G. Goteti, and E. F. Wood (2006), Development of a 50-yr high-resolution global dataset of meteorological forcings for land surface modeling, *J. Clim.*, *19*(13), 3088–3111.

Shi, X., D. Yu, E. D. Warner, X. Pan, G. W. Petersen, Z. G. Gong, and D. C. Weindorf (2004), Soil database of 1:1,000,000 digital soil survey and reference system of the Chinese genetic soil classification system, *Soil Surv. Horiz.*, *45*(4), 129–136, doi:10.2136/sh2004.4.0129.

Shi, Y., K. J. Davis, F. Zhang, and C. J. Duffy (2014), Evaluation of the parameter sensitivities of a coupled land surface hydrologic model at a critical zone observatory, *J. Hydrometeorol.*, *15*(1), 279–299, doi:10.1175/JHM-D-12-0177.1.

Tapley, B. D., S. Bettadpur, M. Watkins, and C. Reigber (2004), The gravity recovery and climate experiment: Mission overview and early results, *Geophys. Res. Lett.*, *31*, L09607, doi:10.1029/2004GL019920.

van der Velde, Y., N. Vercauteren, F. Jaramillo, S. C. Dekker, G. Destouni, and S. W. Lyon (2014), Exploring hydroclimatic change disparity via the Budyko framework, *Hydrol. Processes*, *28*(13), 4110–4118, doi:10.1002/hyp.9949.

Vogel, R. M., and I. Wilson (1996), Probability distribution of annual maximum, mean, and minimum streamflows in the United States, *J. Hydrol. Eng.*, *1*(2), 69–76, doi:10.1061/(ASCE)1084-0699(1996)1:2(69).

Wang, A., and X. Zeng (2011), Sensitivities of terrestrial water cycle simulations to the variations of precipitation and air temperature in China, *J. Geophys. Res.*, *116*, D02107, doi:10.1029/2010JD014659.

Wang, K., and R. E. Dickinson (2012), A review of global terrestrial evapotranspiration: Observation, modeling, climatology, and climatic variability, *Rev. Geophys.*, *50*, RG2005, doi:10.1029/2011RG000373.

Wilson, M. F., A. Henderson-Sellers, R. E. Dickinson, and P. J. Kennedy (1987), Sensitivity of the Biosphere–Atmosphere Transfer Scheme (BATS) to the inclusion of variable soil characteristics, *J. Clim. Appl. Meteorol.*, *26*, 341–362, doi:10.1175/1520-0450(1987)026<0341:SOTBTS>2.0.CO;2.

Wood, E. F., S. D. Schubert, A. W. Wood, C. D. Peters-Lidard, K. C. Mo, A. Mariotti, and R. S. Pulwarty (2015), Prospects for advancing drought understanding, monitoring, and prediction, *J. Hydrometeorol.*, *16*(4), 1636–1657, doi:10.1175/JHM-D-14-0164.1.

Wu, S., Y. Yin, D. Zheng, and Q. Yang (2006), Moisture conditions and climate trends in China during the period 1971–2000, *Int. J. Climatol.*, *26*(2), 193–206, doi:10.1002/joc.1245.

Xia, Y., J. Sheffield, M. B. Ek, J. Dong, N. Chaney, H. Wei, J. Meng, and E. F. Wood (2014), Evaluation of multi-model simulated soil moisture in NLDAS-2, *J. Hydrol.*, *512*, 107–125, doi:10.1016/j.jhydrol.2014.02.027.

Xia, Y., M. B. Ek, Y. Wu, T. Ford, and S. M. Quiring (2015), Comparison of NLDAS-2 simulated and NASMD observed daily soil moisture. Part II: Impact of soil texture classification and vegetation type mismatches, *J. Hydrometeorol.*, *16*(5), 1981–2000, doi:10.1175/JHM-D-14-0097.1.

Xue, Y., P. J. Sellers, J. L. Kinter, and J. Shukla (1991), A simplified biosphere model for global climate studies, *J. Clim.*, *4*(3), 345–364, doi:10.1175/1520-0442(1991)004<0345:ASBMFG>2.0.CO;2.

Yang, Z.-L., et al. (2011), The community Noah land surface model with multiparameterization options (Noah-MP): 2. Evaluation over global river basins, *J. Geophys. Res.*, *116*, D12110, doi:10.1029/2010JD015140.

Zhang, L., W. R. Dawes, and G. R. Walker (2001), Response of mean annual evapotranspiration to vegetation changes at catchment scale, *Water Resour. Res.*, *37*, 701–708, doi:10.1029/2000WR900325.

Zheng, D., R. Van der Velde, Z. Su, J. Wen, X. Wang, M. J. Booij, A. Y. Hoekstra, S. Lv, Y. Zhang, and M. B. Ek (2016), Impacts of Noah model physics on catchment-scale runoff simulations, *J. Geophys. Res. Atmos.*, *121*, 807–832, doi:10.1002/2015JD023695.